

Uncertainty Sources in WorldSID-50M Dummy

Stefan Kronwitter¹, Karin Birkefeld¹, Markus Kösters¹

¹Dr. Ing. h.c. F. Porsche AG

1 Introduction

Full vehicle crash tests are never fully identical in terms of their results, even when conducted with the same configuration. This variability arises from the existence of a diverse set of uncertain input parameters, which induces uncertainty in the relevant quantities of interest (QoI). The classical engineering approach, dealing with scattering system behavior and QoI, is to introduce safety factors and thus ensuring the system's robustness with respect to the adherence of performance-relevant criteria. However, using this strategy within the vehicle safety design process carries the risk that the margins to specific limits might be exceeded in initial hardware tests.

As an extension of the standard development process, the robustness of components up to and including the full vehicle safety system can be virtually assessed [1, 2, 11, 14]. In later development stages, wherein a substantial number of epistemic uncertainties in design parameters have been resolved or transformed, resulting in a dominance of aleatoric uncertainties, probabilistic forward uncertainty quantification (UQ) methods can be utilized for robustness assessment. There exists a variety of UQ methodologies, from classic but less efficient methods such as Monte Carlo simulations to more efficient surrogate-model-based approaches [3, 9, 8]. Within the UQ framework, an essential step is the identification, characterization, and aggregation of uncertainty sources in the input of the computational model [10]. The uncertain input parameters are represented using appropriate probability distributions, and the resulting stochastic space is defined through the joint probability density function of all uncertain parameters. These input uncertainties are then propagated to the QoI by calculation of realizations drawn from the input probability distribution through the finite element model.

Within the domain of occupant safety, the primary QoI are the load signals captured by anthropometric test devices (ATDs). These signals are influenced by variations of the restraint systems, the interior, the structure, and the load case conditions, but also by variations originating from the ATD itself. These can be e.g., uncertainty in the initial seating position or uncertainty in parameters affecting the performance of an ATD. The objective of this study is to identify and characterize relevant scattering physical input parameters inherent to the ATD itself and to investigate their impact on responses, exemplified by the WorldSID 50th percentile adult male dummy. Given the significance of this task in conducting virtual robustness assessments of occupant safety systems, the characterized set of uncertain input parameters can be used in such studies. Furthermore, the simulation-based analysis of crash tests can be enhanced by using a WorldSID model adapted to the dummy used in the test.

The performance of the WorldSID is regularly assessed through certification tests, wherein the QoI are solely influenced by the inherent variations in the dummy and the testing conditions. The results of these tests contain the actual observed variations in ATD responses and can be utilized for two distinct purposes. First, through data analyses of these results, highly variable responses can be identified, and insights can be provided, which input parameters might cause the uncertainty in the ATD signals. Second, the test results can be used for validation of simulation models, where the effect of the identified uncertain input parameters is examined. The analysis of the hardware certification tests is presented in Section 2. Based on this, the uncertainty in the geometries of the rib assemblies has been found to be influential and is characterized in Section 3. The effect of the identified set of uncertain input parameters is studied and validated in Section 4.

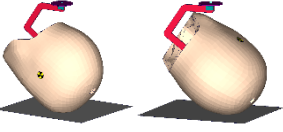
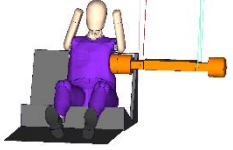
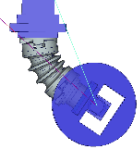
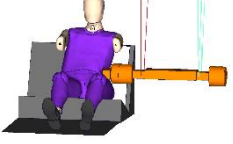
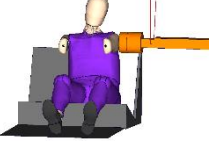
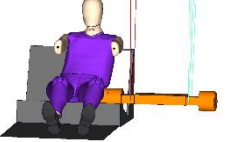
2 Analysis of hardware certification tests

The performance of various body regions of the WorldSID-50M dummy is assessed through dynamic certification tests [6]. Table 1 provides an overview and brief description of all certification tests for each body region. For the validation of the performance of specific body regions, a tolerance-based approach is employed in all certification tests, not only for the WorldSID but also for many other types of ATDs as well.

Subsequently, emphasis is put on three full body tests, namely the shoulder, thorax, and abdomen certification test. In all these tests, a pendulum hits the specific body region at a permissible velocity range of 4.3 ± 0.1 m/s and the energy input remains within defined limits. Also, the seating position of the ATD on the validation bench as well as the impact location of the pendulum shall be in a predefined tolerance range. In the shoulder test, only two load signals are assessed: the time history of the

pendulum force and the shoulder rib deflection. Their maximum values (permissible range for pendulum force: 2.6 to 3.3 kN, for shoulder deflection: 35 to 45 mm) as well as the time delay between the two peak values (which must exceed 15 ms) are utilized for validation [6]. However, the shoulder force along the y-axis is not considered in this test, despite its maximal value serving as a performance criterion in side impact crash tests. Another complication in this test is that the arm, which is hit by the pendulum, establishes two load paths, a main one on the shoulder rib and a second one to the first thoracic rib.

Table 1: Overview and brief description of all necessary certification tests for the WorldSID dummy.

| | | | |
|---|---|---|---|
| <p>Head</p> <ul style="list-style-type: none"> - Lateral head drop for each side - Frontal head drop |  | <p>Thorax</p> <ul style="list-style-type: none"> - Lateral impact test for each side |  |
| <p>Neck</p> <ul style="list-style-type: none"> - Lateral flexion test for each side - Torsion test in each direction of rotation |  | <p>Abdomen</p> <ul style="list-style-type: none"> - Lateral impact test for each side |  |
| <p>Shoulder</p> <ul style="list-style-type: none"> - Lateral impact test for each side |  | <p>Pelvis</p> <ul style="list-style-type: none"> - Lateral impact test for each side |  |

Due to the relatively large tolerance ranges, the test setup, and the fact that crucial variables are not evaluated, there exists considerable space for uncertainty in the performance of the shoulder assembly and in the corresponding load signals. Similar large tolerance ranges are also found in the thorax and abdomen tests. By data analysis of recent hardware certification tests, the variability observed in the relevant responses in the hardware tests is investigated. Statistical metrics for the peak values obtained from these shoulder, thorax, and abdomen tests can be found in Tables 2, 3, and 4. The time-history curves of the responses for the shoulder test are illustrated in Fig. 1.

For the shoulder test, the pendulum force and the shoulder rib deflection exhibit a moderate level of variation, whereas the shoulder force and the first thoracic rib deflection display higher variance. The Range of the shoulder force, measuring 0.46 kN, is significant, particularly in view of the threshold of 3 kN in the Pole Side Impact [13]. The observed variation for pendulum force and rib deflection aligns comparably with the repeatability and reproducibility studies in the ISO standard [5] and by the NHTSA [7]. However, the shoulder force within the investigated dataset demonstrates a significantly elevated level of variability compared to findings of the NHTSA. In case of the thorax test, the T4 and T12 accelerations along the y-axis show high variability. The thoracic rib deflections, with an approximate Coefficient of Variation (CoV) of 5 %, demonstrate a moderate level of variation. These results are consistent with those presented in [5, 7]. Concerning the abdomen test, both abdominal rib deflections and the T12 acceleration reveal lower levels of variation compared to the observed in the thorax tests, a trend that also concurs with the findings in [5, 7]. Overall, higher levels of variability are evident in the shoulder and thorax tests, which is why these are closer examined in Section 4.

Table 2: Mean, CoV and Range (distance between maximum and minimum value) for peak values of relevant responses in the hardware shoulder tests.

| Response | Mean | CoV | Range |
|---|---------|--------|---------|
| Pendulum force | 2.97 kN | 4.98 % | 0.62 kN |
| Shoulder force y-axis | 1.62 kN | 7.90 % | 0.46 kN |
| Shoulder rib deflection | 36.6 mm | 4.49 % | 6.0 mm |
| 1 st thoracic rib deflection | 18.8 mm | 8.68 % | 5.3 mm |

Table 3: Statistical metrics for peak values of relevant responses in the hardware thorax tests.

| Response | Mean | CoV | Range |
|---|---------|--------|---------|
| Pendulum force | 3.73 kN | 1.74 % | 0.24 kN |
| 1 st thoracic rib deflection | 35.4 mm | 5.38 % | 5.9 mm |
| 2 nd thoracic rib deflection | 36.1 mm | 3.93 % | 5.6 mm |
| 3 rd thoracic rib deflection | 34.2 mm | 5.01 % | 5.7 mm |
| T4 acceleration y-axis | 15.2 g | 6.59 % | 4.1 g |
| T12 acceleration y-axis | 16.3 g | 9.85 % | 4.9 g |

Table 4: Statistical metrics for peak values of relevant responses in the hardware abdomen tests.

| Response | Mean | CoV | Range |
|--|---------|--------|---------|
| Pendulum force | 3.05 kN | 2.65 % | 0.37 kN |
| 1 st abdominal rib deflection | 34.3 mm | 3.43 % | 3.8 mm |
| 2 nd abdominal rib deflection | 31.8 mm | 4.12 % | 4.2 mm |
| T12 acceleration y-axis | 17.6 g | 5.42 % | 3.8 g |

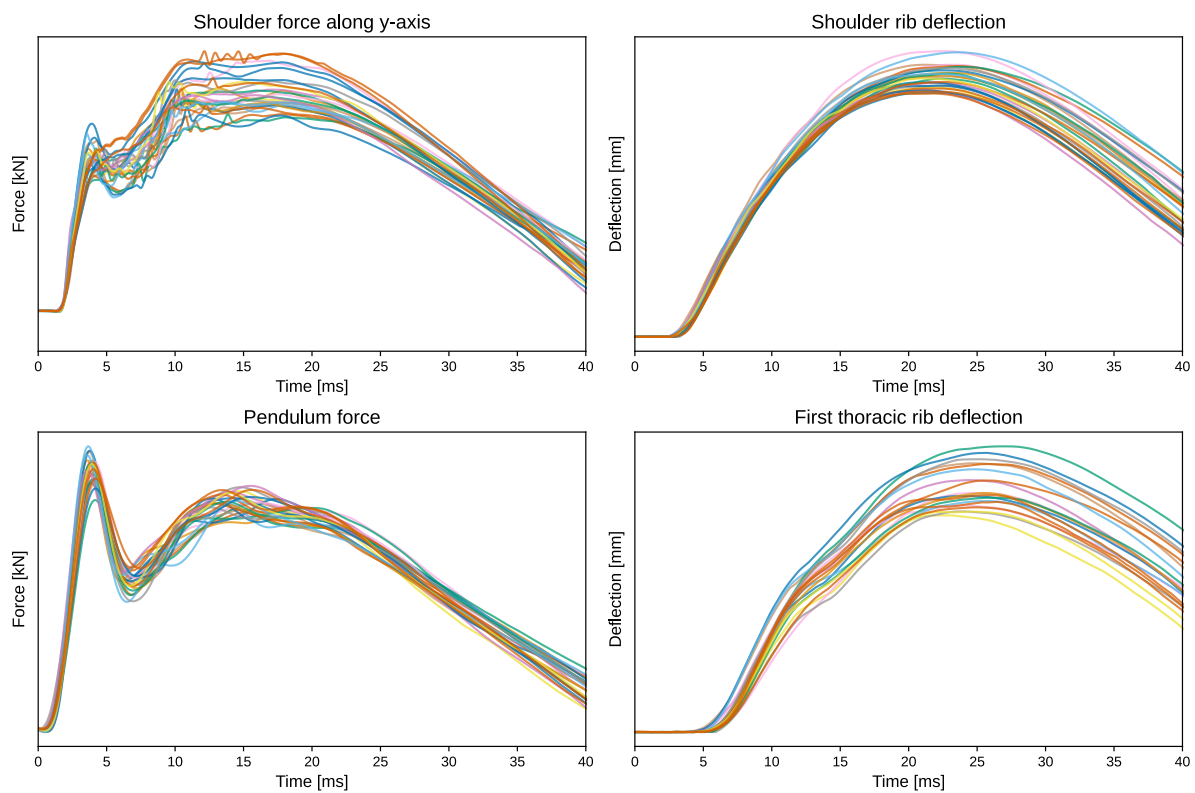


Fig.1: Relevant responses for the shoulder test from the available hardware dataset.

To gain a deeper understanding of the variability in the hardware test results, the time-history curves are studied using Principal Component Analysis (PCA) [12]. As a linear data reduction technique, PCA reduces in this application the time-histories from all tests corresponding to a specific response onto a lower dimensional space, while preserving the most variance of the original dataset in the reduced dimensions. The dimension capturing the highest variance in the reduced space is referred to as the first principal component (PC 1). This nomenclature continues for subsequent dimensions. Fig. 3 illustrates the PCA results for the shoulder force along y-axis in case of the shoulder tests. In the scatter plot depicted on the left-hand side, the first two principal components for all shoulder force responses, as well as the lifecycle of an individual WorldSID, are presented. On the right-hand side, the respective reconstructions of these two components are illustrated. Analyzing the depicted lifecycle of the individual dummy reveals a shift in the characteristic of the shoulder force, as represented by the distance within the principal subspace, attributed to the replacement of the shoulder rib. In contrast, variations between tests featuring the same rib are not as pronounced. Rhule and Stricklin substantiate this observation [7]. In their report, the individual WorldSIDs exhibit notably lower CoVs in the responses for the shoulder test, as compared to the overall CoVs across all investigated dummies. Consequently, it can be deduced

that the installed rib significantly impacts not only the shoulder force but also potentially affects other shoulder responses. Considering the upper body's composition of three thoracic ribs and two abdominal ribs on each side, a comparable influence is anticipated across all upper body responses.

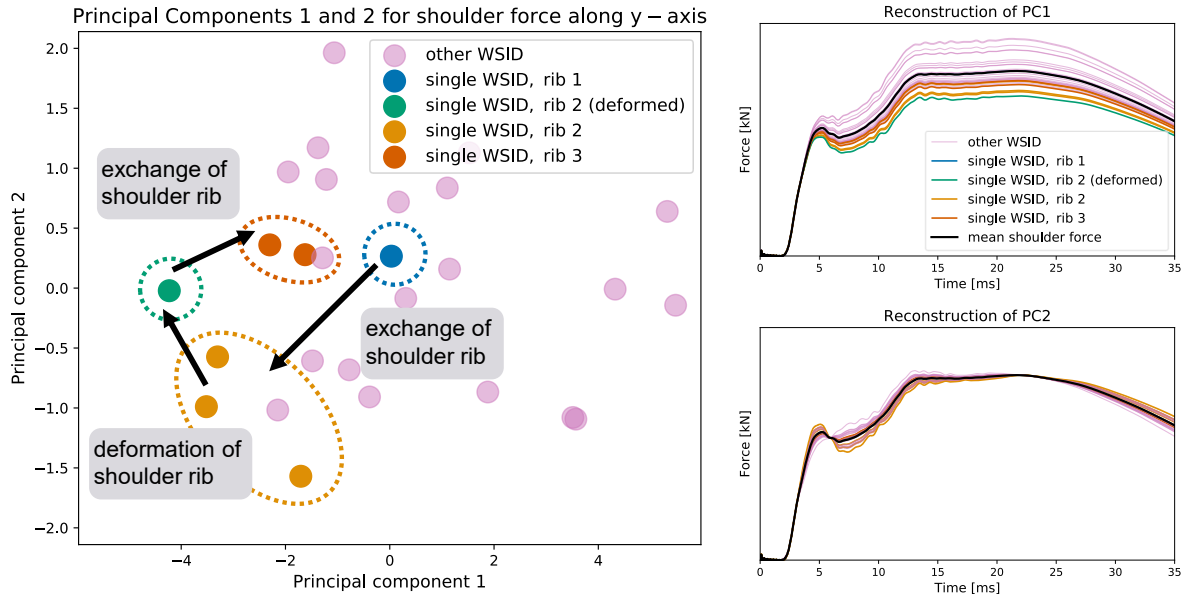


Fig.2: Principal Component Analysis for the shoulder force along y-axis. Scatter plot of PC 1 (explains 81.1 % of total variance in the original dataset) and PC 2 (explains 8.9 %) with the lifecycle of an individual WorldSID (left). Reconstruction of PC 1 (upper right) and PC 2 (lower right).

3 Uncertainty in geometry of the rib assemblies

As shown in the previous section, the variations in the responses in the shoulder, thorax, and abdomen tests are dependent on the characteristics of the installed rib. Furthermore, as depicted in Fig. 6, the shoulder force response is hardly influenced by changes in the pendulum velocity. In contrast, the shoulder rib deflection depends on the velocity and thereby on the energy input. Hence, the shoulder force signal is mainly governed by the stiffness of the shoulder rib and the arm, thereby being affected by the material properties and the geometry of the individual shoulder rib assembly. Consequently, the geometric variations exhibited by the rib assemblies are quantified as follows.

The assembly of a rib consists of two rib sheets made of nitinol alloy with an additional third sheet for the shoulder rib. Two damping materials are glued to the inner side of the inner rib, as illustrated in Fig. 3. When considering influential sources of variability for the rib stiffness, significant importance is attributed to the wall thicknesses of each part. Utilizing measurement data from three distinct rib sets, the deviations in wall thicknesses for each component are characterized through probability distributions. Notably, among the individual rib types (shoulder, thorax, abdomen), no significant variations in nitinol sheet thicknesses are apparent. As a result, these thicknesses are modeled using a single random variable. In contrast, the wall thicknesses of the damping materials differ across the rib types, thereby necessitating their separate assessment. All four thicknesses can be assumed to follow a normal distribution, as partly depicted in Fig. 4 and Table 5. Additionally, the Table compares the normal distributions with the nominal parameterization of the Beta WorldSID Model Version 8 by DYNAMore.

Table 5: Comparison of inferred normal distributions (parameters: mean value and standard deviation) and nominal parameters for the Beta WorldSID model

| Parameter Name | Beta WorldSID Model [mm] | Normal distributions [mm] |
|--------------------------------|--------------------------|---------------------------|
| Inner and outer rib | 1.57 | $\mathcal{N}(1.62, 0.05)$ |
| Rib doubler | 2.20 | $\mathcal{N}(1.62, 0.05)$ |
| Shoulder rib damping material | 4.80 | $\mathcal{N}(4.93, 0.10)$ |
| Thoracic rib damping material | 3.00 | $\mathcal{N}(3.93, 0.52)$ |
| Abdominal rib damping material | 4.80 | $\mathcal{N}(4.43, 0.36)$ |

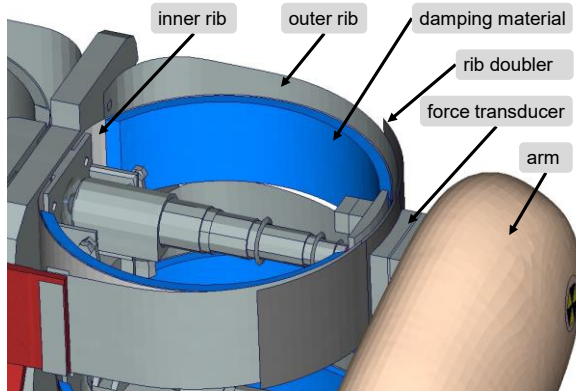


Fig.3: Design of the shoulder rib

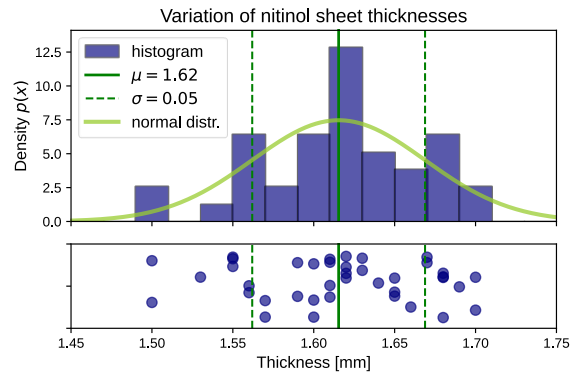


Fig.4: Scatter plot, histogram and inferred normal distribution of the nitinol sheet thicknesses

The rib doubler shows greater thickness in the model, whereas the inner and outer rib has slightly smaller thicknesses than evident in the measurement data. The damping material thicknesses for the thoracic and abdominal ribs demonstrate considerably higher variance compared to that of the shoulder. This can be attributed to the experimental setup of the thorax and abdomen test, where three respectively two ribs are subjected to parallel loading. By combining ribs of varying stiffness, the tolerance limits for the evaluated responses can be adhered to as with ribs of similar stiffness, consequently resulting in this higher variance of the damping material thicknesses. Furthermore, the damping material thicknesses display inhomogeneity, possibly originating from eccentricity introduced during the milling process of the cylindrical shape at random angles. This eccentricity can also be regarded as normal distributed ($\sim \mathcal{N}(0.14 \text{ mm}, 0.05 \text{ mm})$).

4 Validation

This section examines whether and to what extent the identified and characterized uncertainty in the rib geometries influence the uncertainty in the upper body responses. A two-fold approach is used to validate this hypothesis. First, certification tests are simulated by individually adjusting the rib geometries of the WorldSID model and the test parameters. Then the resulting signals are compared with those of the corresponding hardware tests to quantify whether the accurate representation of the rib geometries translates into a better fit of the responses. In the second approach, stochastic simulations are conducted to propagate the uncertainty in the input parameters forward to the ATD signals. The resulting uncertainty of the virtual sample is assessed in relation to the observed uncertainty in hardware tests. In both validation studies, we investigate the thorax and the shoulder test. The simulation models for the certification tests were kindly provided by DYNAMore, wherein the Beta Version of the new WorldSID Version 8 was utilized.

4.1 Simulation with individually adapted WorldSID models

For two out of the three rib sets that were measured, associated hardware tests are available, which were simulated. The rib thicknesses for each body region are detailed in Table 6 and have been incorporated into the WorldSID model. For each of the two rib sets, one thorax test is available. Regarding the shoulder tests two tests with different impact velocities exist for rib set 1 and one test for rib set 2.

In Fig. 5, the relevant responses of the thorax tests, the three thoracic rib deflections and the pendulum force, are depicted for the nominal WorldSID model, the adjusted models, and the corresponding hardware. In both hardware tests, the pendulum impacted with 4.32 m/s, as was set in the simulations as well. It is evident that by modifying the rib geometry, a significantly improved fit is achieved across all four responses in comparison to the nominal model. The responses for both adapted models are nearly identical despite the distinct thicknesses. This can be attributed to the parallel loading of the three thoracic ribs since the overall rib stiffness governs the characteristics of the pendulum force and the three rib deflections. In case of the first thoracic rib deflection, the adjusted models slightly underestimate the maximum value by 1.5 mm for rib set 1 and by 0.8 mm for rib set 2. For the second rib, the adjusted models predict a maximum deflection, which is off by around 1 mm for each of the tests. For the third rib, the adjusted model for rib set 1 matches the hardware test quite well, but in case of rib set 2 there is an overestimation of 2 mm. Regarding the pendulum force, its time-history is first overestimated, followed by an underestimation in the 17 to 25 ms interval. In sum, the predictive accuracy has been improved by the adjustment of the rib geometries compared to the nominal model for the thorax tests.

Table 6: Rib thicknesses of the measured rib sets corresponding to the hardware tests. For the damping material the mean value of the wall thickness is given.

| Rib set number | Body region of the rib | Damping material [mm] | Nitinol sheet of inner rib [mm] | Nitinol sheet of outer rib [mm] | Nitinol sheet of rib doubler [mm] |
|----------------|------------------------|-----------------------|---------------------------------|---------------------------------|-----------------------------------|
| 1 | shoulder | 4.90 | 1.60 | 1.68 | 1.50 |
| 1 | first thorax | 4.45 | 1.55 | 1.68 | - |
| 1 | second thorax | 2.90 | 1.70 | 1.68 | - |
| 1 | third thorax | 4.50 | 1.50 | 1.55 | - |
| 2 | shoulder | 4.85 | 1.65 | 1.60 | 1.65 |
| 2 | first thorax | 3.92 | 1.61 | 1.64 | - |
| 2 | second thorax | 4.05 | 1.55 | 1.65 | - |
| 2 | third thorax | 4.43 | 1.57 | 1.62 | - |

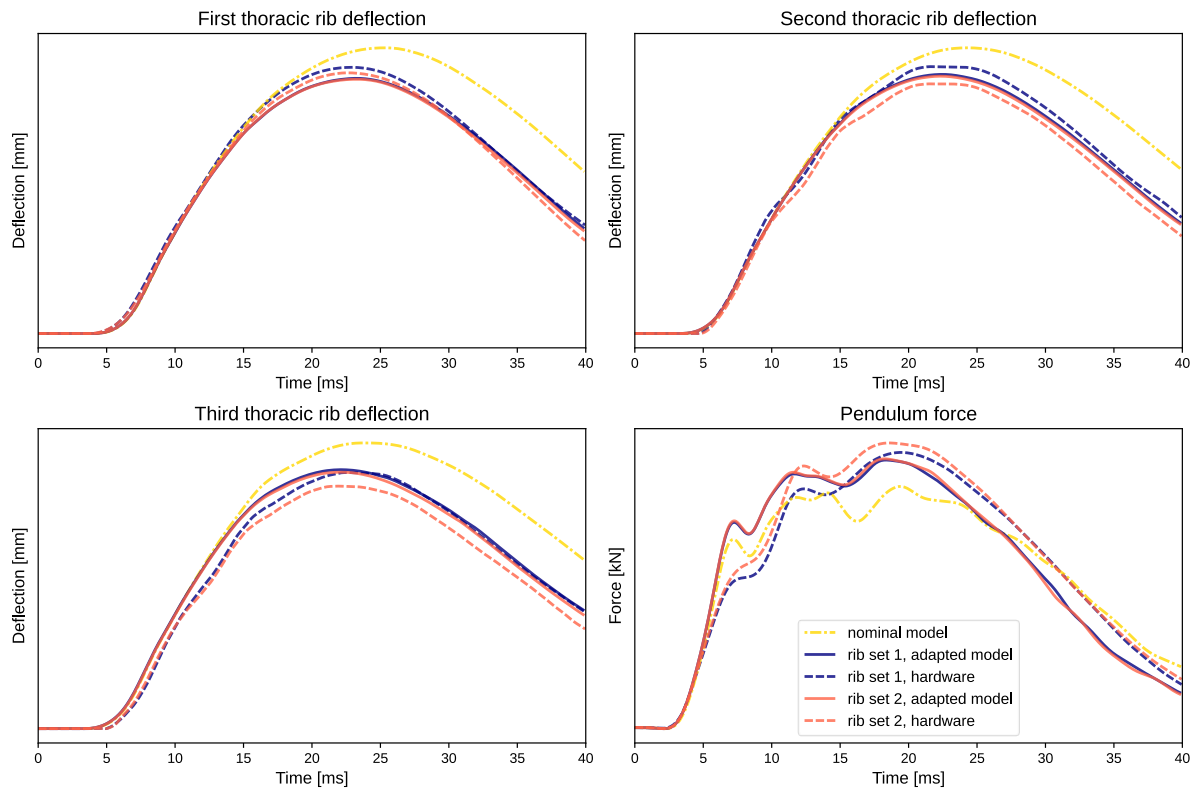


Fig.5: Responses of simulated and associated hardware thorax tests for the two measured rib sets.

The two shoulder tests associated with rib set 1 exhibit differing impact velocities ($v_1 = 4.3$ m/s, $v_2 = 4.025$ m/s). The relevant ATD responses, the shoulder force along the y-axis and the shoulder rib deflection, are outlined in Fig. 6. Both, the nominal, and the adjusted model, show good agreement with the two hardware tests across both signals. The modifications in the rib geometry lead to only marginal changes in the responses, primarily because of the minor deviation in damping material thickness from the nominal model. The differences in the nitinol sheet thicknesses balance out in such a way (higher thickness for the inner and outer rib, considerably lower thickness for the doubler) that the geometric stiffness of the rib remains nearly unaltered. In case of rib set 2, the initial agreement between responses of the nominal model and the hardware test is not as good as in comparison to rib set 1, as depicted in Fig. 7. Due to the rather similar thickness changes from the nominal to the adjusted model, as in rib set 1, these adaptations result in marginal changes in the curves, thereby not contributing to an improved alignment with the hardware test. The second force rise initiates slightly earlier in the hardware test, and the force level in the time interval from 10 to 20 ms is higher than in the two simulation models. The shoulder rib deflection is overestimated by both simulation models, with a maximum deviation of 4 mm compared to the hardware test. This phenomenon could potentially be attributed either to different arm characteristics or to substantial variations in the material behavior within the shoulder rib assembly, in contrast to the utilized material model in the simulation.

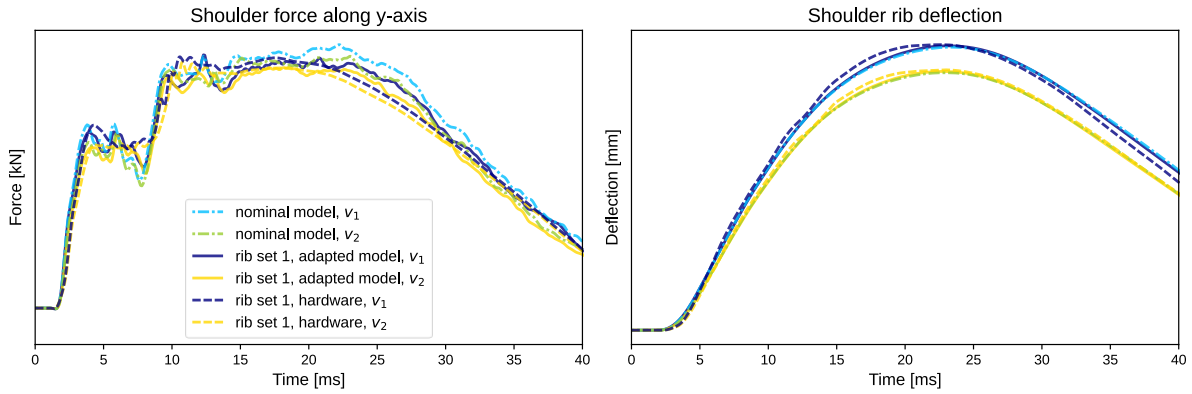


Fig.6: Responses of simulated and associated hardware shoulder tests for the rib set 1.

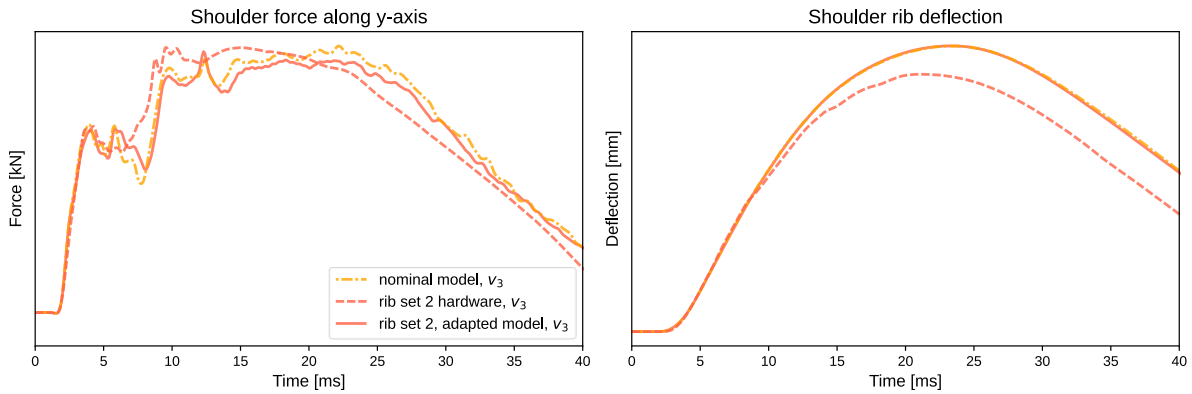


Fig.7: Responses of simulated and associated hardware shoulder test for the rib set 2.

4.2 Stochastic Simulations

Within the two stochastic simulations, the rib geometries, as well as the impact location and the velocity of the pendulum, were represented as uncertain input parameters. The thicknesses of the nitinol sheets and the damping materials for the shoulder, thoracic, and abdominal ribs are modeled as normally distributed random variables, as described in Section 3. Additionally, random eccentricities were incorporated into the thicknesses of the damping materials. The impact location and velocity are modeled with uniform probability distributions, with limits of ± 10 mm around the nominal impact location for both the x- and y-directions. The boundaries for the pendulum velocity are set to the permissible range of 4.2 to 4.4 m/s. The described random field is discretized using Advanced Latin Hypercube Sampling [4], and the realizations are incorporated into a parameterized version of the baseline certification test models. For both stochastic simulations, a sample size of 50 is utilized. Furthermore, in the shoulder test, the yoke angle of the arm is discretely spread in a uniform manner, ranging from -2° to $+2^\circ$ in 1° steps. This is done to effectively simulate the varying interaction between the arm and the first thoracic rib.

The time histories of the thoracic rib deflections and the pendulum force for both the stochastic simulation and the hardware thorax tests are depicted in Fig. 8. The rib deflections in the stochastic simulation show a good alignment with the experimental curves. The time histories of the pendulum force are over-predicted in the simulations within the time span of 5 to 12 ms, while from 15 ms onwards they are underestimated, a trend that was also observed in the simulations with individually adapted WorldSID models. Furthermore, upon comparing the maximum thoracic rib deflections from the stochastic simulation with those from the hardware tests, see Fig. 9, it becomes evident that by incorporating the uncertainty in the rib geometries within the permissible pendulum velocity range, the simulation results adeptly reflect the stochastic characteristics of the maximum values in the hardware tests. This observation is also valid for the third thoracic rib, where the mean values of both sets differ by a mere 0.1 mm, but the hardware tests exhibit a slightly higher variance ($CoV_{hardware} = 4.9\%$, $CoV_{stoch. sim.} = 3.7\%$).

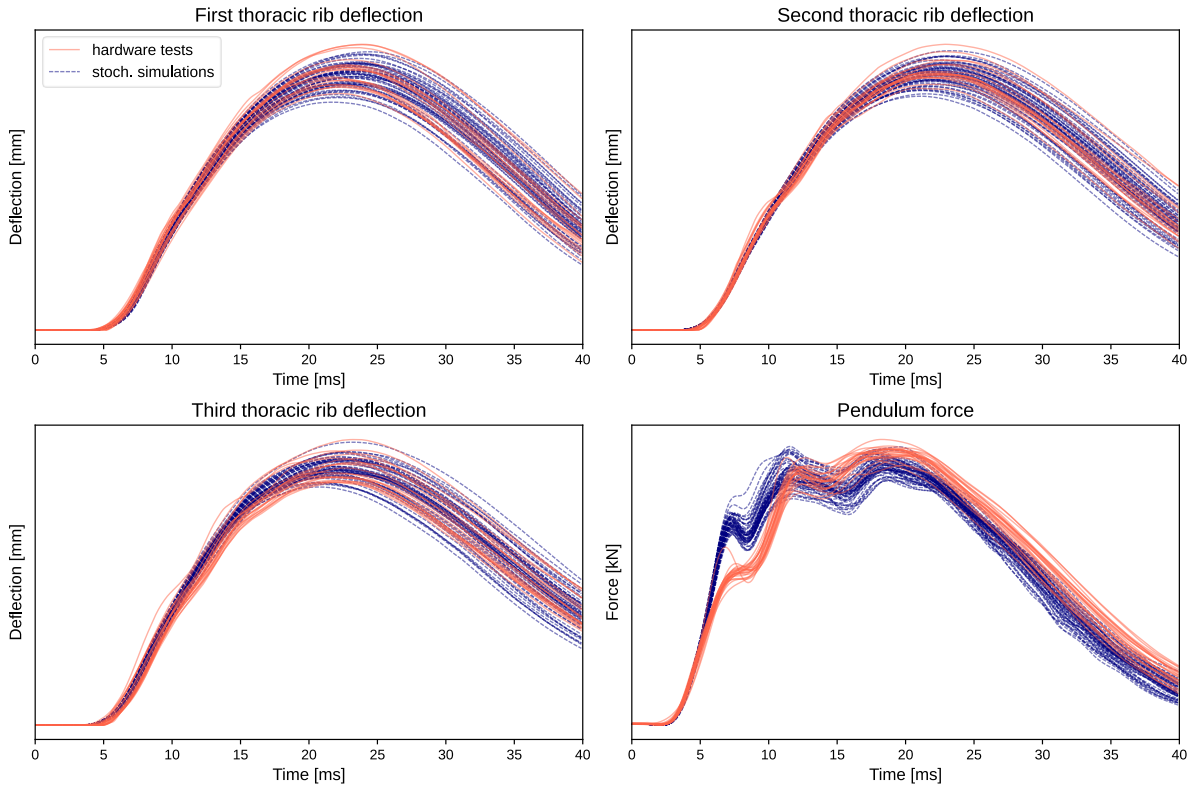


Fig.8: Responses of the stochastic simulation and hardware thorax tests.

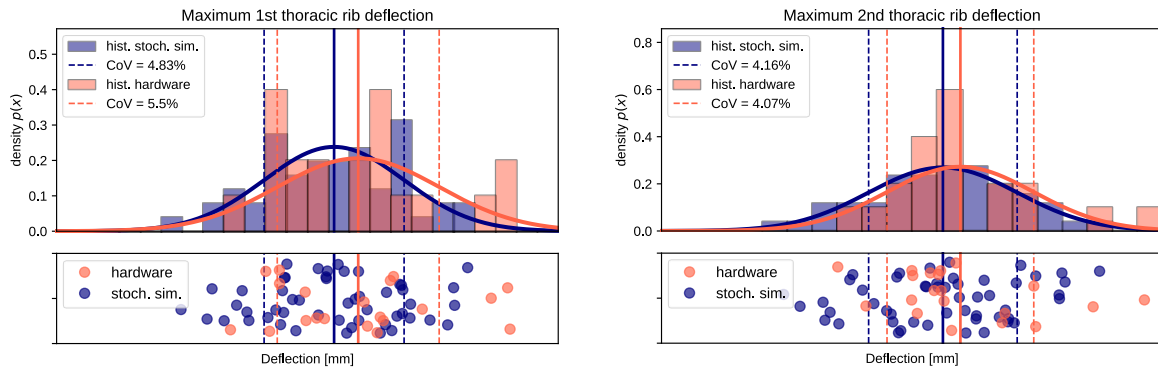


Fig.9: Histograms, inferred normal distributions and scatter plots of the maximum rib deflections of the first (left) and second thoracic rib (right) for the stochastic simulation and the hardware tests.

In contrast to the thorax test, the agreement in responses between the stochastic simulation and the hardware tests in the shoulder test is not as pronounced, as depicted in Fig. 10. In the stochastic simulation, the mean level of the shoulder force along y-axis tends to align with the lower scatter range of the hardware tests, with a reduced scatter range. This observation is further underscored by evaluating the maximum values, see Fig. 11. The mean value for the simulations deviates by 0.05 kN, and the coefficient of variation is also significantly reduced ($CoV_{hardware} = 8.25\%$, $CoV_{stoch. sim.} = 2.84\%$). The observed underestimation in shoulder force yields an upward bias in the estimation of the shoulder rib deflection in the stochastic simulation. The mean value of the maximum deflection is 4.5 mm larger than the value derived from the hardware tests. However, the discrepancy in the CoV is moderate. The uncertainty in the responses observed in the shoulder hardware tests could only be replicated to a limited extent in the stochastic simulation. One possible explanation is the limited number of measured shoulder ribs, potentially leading to an inferred normal distribution that might not fully align with the underlying probability distribution of the population. Additionally, unaccounted-for, and undisclosed variations in arm characteristics and rib material properties might also contribute significantly to this divergence.

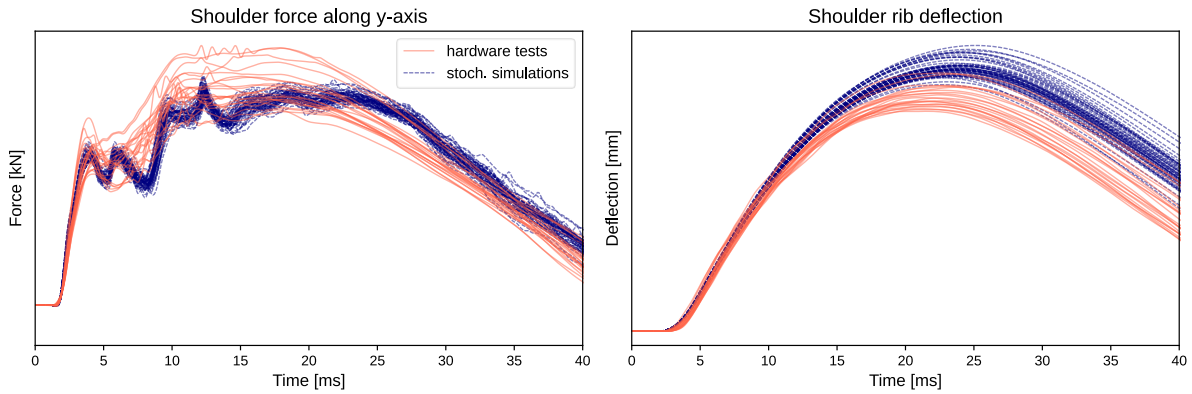


Fig.10: Responses of the stochastic simulation and hardware shoulder tests.

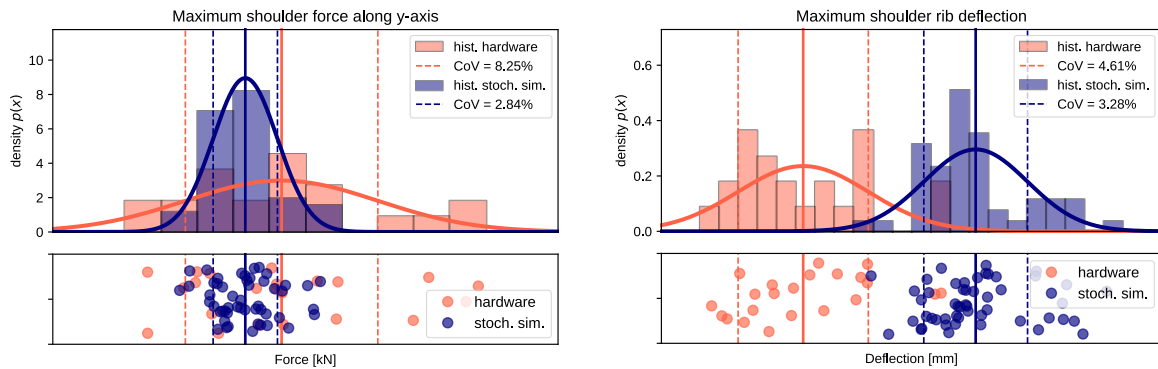


Fig.11: Histograms, inferred normal distributions and scatter plots of the maximum shoulder force (left) and maximum shoulder rib deflection (right) for the stochastic simulation and the hardware tests.

5 Summary

As defined in the ISO standard for the WorldSID dummy, the responses of specific body regions within the certification tests are allowed to show variability within specific tolerance ranges. Through this analysis and insights from other literature, it has become evident that the maximum values of the relevant responses in hardware tests cover these tolerance ranges to a high degree. This variability relies partly on the currently installed components in the dummy, as illustrated by the changing shoulder force characteristics resulting from shoulder rib replacements.

Based on these insights, the geometric differences across three sets of ribs, particularly the variations in wall thicknesses, were identified as potentially influential parameters and thus were measured, given their substantial impact on the rib stiffness. These thicknesses can be represented by normal distributions. The determined mean values of the nitinol sheet thicknesses and of the damping materials partly deviate from the nominal values of the WorldSID model by DYNAMore.

Two approaches were used to validate whether the characterized variations in rib geometries provide an explanation for the observed uncertainty in the hardware test responses. First, certification tests were simulated by individually adjusting the rib geometries of the WorldSID model. In the second approach, stochastic simulations were conducted. In the case of the thorax test, the variations in rib geometries appear to be the primary influencing factors, as demonstrated by the notable agreement observed in both validation approaches between simulations and their corresponding hardware tests. Furthermore, the inferred probability distributions of the uncertain input parameters seem to reflect the population. For the shoulder test, the variations in rib geometry seem to exert a partial impact on the relevant responses, as evidenced by the simulation results displaying differences in both mean value and variance for each metric. This might be attributed to the limited number of measured ribs used for inferring the probability distribution of the damping material thickness of the shoulder rib, or to the existence of significant epistemic uncertainty related to arm characteristics or material properties.

Findings from this study can be used to improve the simulation-based analysis of crash tests by using a WorldSID model adapted to the dummy used in the test. Furthermore, the characterized set of uncertain input parameters can be applied in virtual robustness assessments of occupant safety systems.

6 Literature

- [1] Andricevic N., Duddeck F., and Hiermaier S.: "A novel approach for the assessment of robustness of vehicle structures under crash", *International Journal of Crashworthiness*, vol. 21, no. 2, 2016, pp. 89–103.
- [2] Brix C. and Tok C. H.: "Robust Design in Occupant Safety Simulation", *SAE International Journal of Transportation Safety*, vol. 1, no. 2, 2013, pp. 241–260.
- [3] Duddeck F. and Wehrle E.: "Recent advances on surrogate modeling for robustness assessment of structures with respect to crashworthiness requirements", 10th European LS-DYNA Conference 2015, Würzburg, Germany.
- [4] Huntington D. E. and Lyrantzis C. S.: "Improvements to and limitations of Latin hypercube sampling", *Probabilistic Engineering Mechanics*, vol. 13, no. 4, 1998, pp. 245–253.
- [5] International Organization for Standardization: "Road vehicles — Design and performance specifications for the WorldSID 50th percentile male side-impact dummy - Part 1: Vocabulary and rationale", ISO 15830-1, Geneva, 2022.
- [6] International Organization for Standardization: "Road vehicles — Design and performance specifications for the WorldSID 50th percentile male side-impact dummy - Part 2: Mechanical subsystems", ISO 15830-2, Geneva, 2022.
- [7] Rhule D. A. and Stricklin J. L.: "Evaluation of the WorldSID 50th percentile male side impact dummy: Qualification and Sled Test Repeatability and Reproducibility", *National Highway Traffic Safety Administration: Report No. DOT HS 813 214*, 2022.
- [8] Rocas M., García-González A., Larráyoiz X., and Díez P.: "Adaptive surrogates of crashworthiness models for multi-purpose engineering analyses accounting for uncertainty", *Finite Elements in Analysis and Design*, vol. 203, 2022.
- [9] Rocas M., García-González A., Larráyoiz X., and Díez P.: "Nonintrusive Stochastic Finite Elements for Crashworthiness with VPS/Pamcrash", *Archives of Computational Methods in Engineering*, vol. 27, no. 4, 2020, pp. 1337–1362.
- [10] Sudret B.: "Polynomial chaos expansions and stochastic finite element methods", *Risk and Reliability in Geotechnical Engineering*, 2015, pp. 265–300.
- [11] Thole C.-A. and Mei L.: "Reasons for Scatter in Crash Simulation Results", 4th European LS-DYNA Users Conference, Ulm, 2003.
- [12] Tipping M. E. and Bishop C. M.: "Probabilistic Principal Component Analysis", *Journal of the Royal Statistical Society: Series B (Statistical Methodology)*, vol. 61, no. 3, 1999, pp. 611–622.
- [13] "Uniform provisions concerning the approval of vehicles with regard to their Pole Side Impact performance: Regulation No. 135", *World Forum for Harmonization of Vehicle Regulations*, 2014.
- [14] Will J., Baldauf H., and Bucher C.: "Robustness Evaluations in Virtual Dimensioning of Passive Passenger Safety and Crashworthiness", 3rd Weimar Optimization and Stochastic Days, Weimar, 2006.